# Glasslike behavior of a hard-disk fluid confined to a narrow channel

J. F. Robinson, M. J. Godfrey, and M. A. Moore
*School of Physics and Astronomy, University of Manchester, Manchester M13 9PL, United Kingdom*
(Received 15 January 2015; published 1 March 2016)

Disks moving in a narrow channel have many features in common with the glassy behavior of hard spheres in three dimensions. In this paper we study the caging behavior of the disks that sets in at characteristic packing fraction $\phi_d$. Four-point overlap functions similar to those studied when investigating dynamical heterogeneities have been determined from event-driven molecular dynamics simulations and the time-dependent dynamical length scale has been extracted from them. The dynamical length scale increases with time and, on the equilibration time scale, it is proportional to the static length scale associated with the zigzag ordering in the system, which grows rapidly above $\phi_d$. The structural features responsible for the onset of caging and the glassy behavior are easy to identify as they show up in the structure factor, which we have determined exactly from the transfer-matrix approach.

DOI: 10.1103/PhysRevE.93.032101

## I. INTRODUCTION

It has been frequently observed that disks moving in a narrow channel can provide useful insights into glassy behavior [1–7]. In a recent paper [6] two of us studied the static and dynamic properties of $N$ disks of diameter $\sigma$, which move in a narrow channel consisting of two impenetrable walls (lines) spaced by a distance $H_d$ such that $1 < H_d/\sigma < 1 + \sqrt{3}/2$ (see Fig. 1).

With channels of this width only nearest-neighbor disks can interact with one another and neighboring disks cannot pass each other so that their ordering is preserved: $0 \leqslant x_1 < x_2 < \cdots < x_N \leqslant L$, where $x_i$ is the position of the center of disk $i$, measured along the channel, and $L$ is the total length available to the disk centers. The coordinate $y_i$ of the $i$th disk is measured from the center of the channel and can vary between $\pm h/2$, where $h = H_d - \sigma$. The packing fraction $\phi$ in our system of disks is defined as

$$\phi = \frac{N\pi\sigma^2}{4H_d L}. \tag{1}$$

Our disks move ballistically, colliding elastically with each other and the channel walls. It is useful for many purposes to regard the disks as being contained within a system of average length $L$ by pistons at the ends of the channel that exert a force $f$ to counteract the momentum transferred by the disks colliding with them. For any finite value of this force, large fluctuations in the $x$ coordinates of the disks cause the time-averaged density of disks to be independent of $x$, so the system is never crystalline. The static equilibrium properties of this simple system can be determined exactly by use of the transfer matrix [6,8–11], but the chief purpose of this paper is to discuss the dynamics. The dynamical properties of our system must be determined from simulations and to this end we have used event-driven molecular dynamics to handle the collisions of the disks with each other and with the channel walls. We find interesting similarities and also some instructive *differences* with the dynamics of three-dimensional glass-forming liquids.

It was found some time ago that in the system of disks in a channel there is a packing fraction $\phi_d \approx 0.48$ above which the dynamics are activated [1]. Similarly, for hard spheres in three dimensions, the relaxation time grows rapidly above a packing fraction of $\approx 0.58$. For a review of this and other features of hard-sphere systems see Ref. [12]. We have also observed that for $\phi > \phi_d \approx 0.48$ zigzag ordering of the disks starts to grow rapidly [6]; that is, the onset of the slow dynamics is connected with the growth of this particular kind of order. There is a long tradition of associating glassy behavior with geometrical features associated with the arrangements of particles around a given particle (see, e.g., [13–17]) and our work on disks in a narrow channel is entirely consistent with these ideas. In our earlier work [6,7] a length scale $\xi$ associated with zigzag order was determined from the decay with $s$ of the correlation function

$$\langle y_i y_{i+s}\rangle \sim (-1)^s \exp(-s/\xi). \tag{2}$$

It is a measure of the number of disks over which the zigzag order, a form of bond-orientational order, persists; it is of the same order as the separation of defects in the zigzag order, where the defects are of the kind illustrated in the top and bottom panels of Fig. 2.

In three-dimensional systems the ordering associated with glassy behavior is complicated [17]. Furthermore, the ordering associated with glassy behavior is not apparent in changes to the structure factor as it is cooled through the glass transition. In Sec. II we calculate the structure factor of our system, defined as

$$S(k_x,k_y) = \frac{1}{N}\sum_{i,j}\langle \exp[ik_x(x_i - x_j) + ik_y(y_i - y_j)]\rangle, \tag{3}$$

at packing fractions close to $\phi_d$ by use of the transfer-matrix formalism and so it is exact to numerical accuracy. It is found to change rapidly near $\phi_d$. This marked difference with the behavior in three dimensions where the structure factor hardly alters near the glass transition indicates that glass behavior in three dimensions must, as suggested in Refs. [13–17], involve higher-order correlations that have little impact on the structure factor, unlike the simple zigzag orientational order of the narrow-channel system.

In Sec. III we study the onset of the slow dynamics that sets in around $\phi_d$. In three dimensions the slow dynamics are normally attributed to the onset of caging behavior where a particle is trapped by its neighbors and this behavior is believed

 

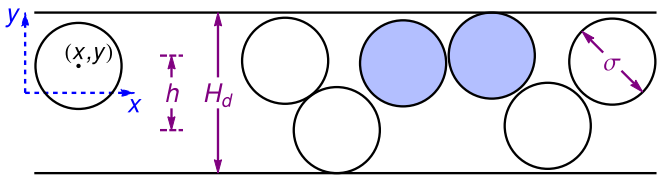


FIG. 1. Illustration of the disk-channel system as in Ref. [6]. The shaded disks represent a defect in the developing zigzag order.

to be captured by the mode-coupling approach. The particle can escape its cage on the $\alpha$-relaxation time $\tau_\alpha$. To determine whether or not caging occurs in our system we have studied the mean-square displacements

$$\Delta^2(t) = \left\langle \frac{1}{N} \sum_{i=1}^{N} |y_i(t) - y_i(0)|^2 \right\rangle, \tag{4}$$

where the average is over different initial states. We find that there is caging of particles in our system, i.e., there is (at large enough packing fractions) a plateau in $\Delta^2(t)$ before its long-time limit is reached. We find that in our system there are

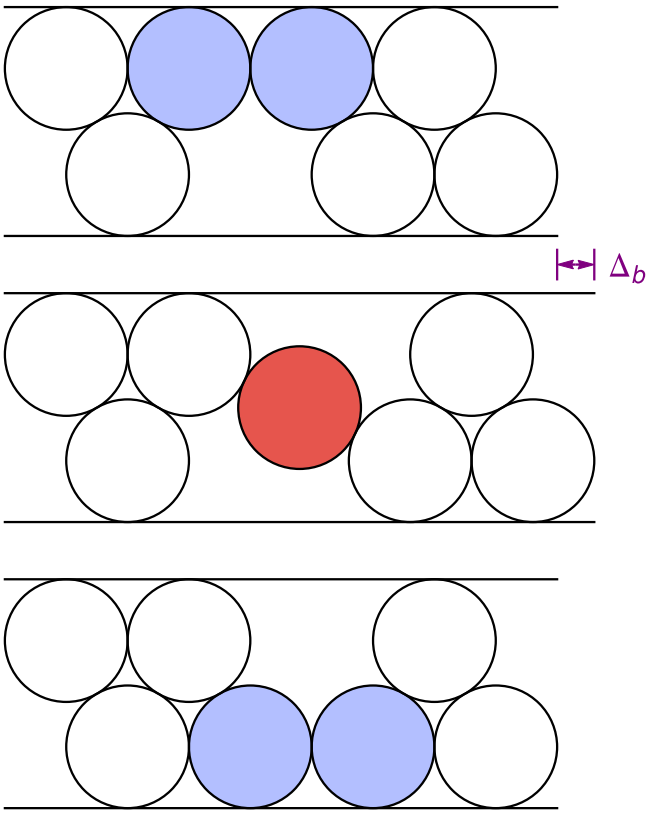


FIG. 2. Transition state for motion of a defect. In the top and bottom diagrams, the two blue-shaded disks are a defect in the zigzag arrangement of disks. The defect can move when one disk crosses the channel by squeezing between its neighbors: The system passes through the transition state shown in the middle diagram to reach the defect state shown in the bottom diagram. In the top diagram the defect involves disks 3 and 4; in the bottom diagram the defect involves disks 4 and 5, when the disks are numbered from the left. The net motion of the defect is to the right and $\Delta_b$ is the extra length needed to allow this motion.

*two* distinct long timescales, which we call $\tau$ and $\tau_D$ following Ref. [6]; we can obtain both of them from the behavior of $\Delta^2(t)$. The smaller of these time scales $\tau$ is the typical time scale for a disk to cross from one side of the system to the other by the process shown in Fig. 2. It marks the time at which the particle starts to escape from its cage or the end of the plateau in $\Delta^2(t)$: In three-dimensional systems this would be called the $\alpha$-relaxation time $\tau_\alpha$. At packing fractions above $\phi_d$, escape from a cage can be regarded as a displacement of a defect in the zigzag ordering of the disks as is also illustrated in Fig. 2. We are able to determine from the simulation the diffusion constant for the movement of such defects. Its dependence on packing fraction is consistent with the general picture of a crossover from fragile glass behavior at low packing fractions to strong glass behavior at high packing fraction, which was investigated previously in Refs. [2,4].

The second long timescale $\tau_D$ is essentially the longest timescale in the system. In equilibrium defects are thermally nucleated in pairs and the defects produced then diffuse and annihilate with each other. It is this process of diffusion with creation and annihilation that takes place on the time scale $\tau_D$. There is a simple relation between $\tau$ and $\tau_D$: $\tau_D \sim \tau\xi^2$ [6]. Note that $\xi$ is the typical distance between defects in equilibrium, so $\xi^2/D$ is the time it would take for a defect to move a distance $\xi$: This gives a diffusion coefficient $D$ for the defects that varies as $1/\tau$ [6]. The long timescale $\tau_D$ is determined from the time at which $\Delta^2(t)$ approaches its equilibrium limit.

A characteristic of glassy dynamics is the appearance of a plateau in the decay of certain time-dependent correlation functions. This plateau eventually decays to zero after the time $\tau_\alpha$, the $\alpha$-relaxation time. The time to reach the plateau is the $\beta$-relaxation time $\tau_\beta$. Correlation functions with this feature have not previously been studied in our narrow-channel system. The existence of a plateau in $\Delta^2(t)$ implies that there will be such a plateau in the decay of

$$R(t) = \frac{1}{N} \sum_i \langle y_i(0) y_i(t) \rangle; \tag{5}$$

at long times $R(t)$ approaches zero. As noted above, our results support a model in which the diffusion of defects leads to equilibrium. In models of this kind, $R(t)$ is expected to decay with a *stretched* exponential form $\exp(-[t/\tau_D]^{1/2})$, where $\tau_D$ is the equilibration time of the system [18].

We have also studied a correlation function related to the $\chi_4(t)$ that has been much studied in three dimensions [15,19,20]. In three dimensions $\chi_4(t)$ rises to a peak at the $\alpha$-relaxation time and then decays to zero as the particles escape their cages. Our $\chi_4(t)$ increases to a constant plateau value as $t$ increases and stays at this value as $t \to \infty$. In this regard the narrow-channel system behaves more like a spin glass than a structural glass [21]. We have also extracted a *dynamical* correlation length $\xi_4(t)$ from a four-point correlation function. In our system as $t \to \tau_D$, $\xi_4$ grows towards the static correlation length $\xi$, which measures the extent of zigzag, i.e., structural, order.

In Sec. II we show how the structure factor can be determined exactly from the transfer-matrix procedure and we demonstrate that it changes rapidly for densities close to

$\phi_d$. Our dynamical studies are in Sec. III. We conclude with a discussion in Sec. IV.

## II. STRUCTURE FACTOR

The structure factor is well known from the part it plays in the scattering of electromagnetic radiation by liquids [22]. It is the Fourier transform of the density-density correlation function and so provides information on the relative positions of scatterers within the system. Like a liquid, our system of disks in a channel has no long-range order (along the channel) for finite values of the longitudinal force $f$; however, unlike in the bulk of a liquid, the short-range order is strongly affected by the presence of confining walls, leading to the zigzag correlations discussed in Sec. I. In this section we show that the structure factor can be calculated essentially exactly for disks in a narrow channel. Our numerical results for the case $h = \sqrt{3}\sigma/2$ show a rapid change in the short-range order for $\beta f\sigma$ in the range 6.5–8, which corresponds to packing fractions $\phi$ in the range 0.45–0.50. This range of packing fractions correlates closely with the onset of activated dynamics, as we discuss later in Sec. III.

In the limit $N \to \infty$, the definition of the structure factor (3) may be rewritten in the form

$$S(k_x,k_y) = \sum_{n=-\infty}^{\infty} S_n = 1 + 2\,\mathrm{Re}\sum_{n=1}^{\infty} S_n, \tag{6}$$

where

$$S_n = \langle e^{i(k_x[x_n-x_0]+k_y[y_n-y_0])}\rangle. \tag{7}$$

At $k_x = 0$, $S(k_x,k_y)$ has a $\delta$-function singularity and the sum on the right-hand side of (6) diverges. As we now show, for $k_x \neq 0$ the sum can be evaluated relatively simply by solving a pair of integral equations. One of these equations is known from the transfer-matrix formalism introduced by Barker [8] and applied by Kofke and Post [9] to the problem of hard disks in a channel. We follow the latter authors in using an ensemble in which the longitudinal force $f$ is constant and we refer the reader to their paper [9] for details.

Let $\psi_n(y)$ be the eigenfunctions of Kofke and Post's integral equation

$$\lambda_n\psi_n(y_1) = \int_{-h/2}^{h/2} e^{-\beta f\sigma_{1,0}}\psi_n(y_0)\,dy_0, \tag{8}$$

where $y_0$ and $y_1$ are the $y$ coordinates of a neighboring pair of disks and $\sigma_{1,0} = [\sigma^2 - (y_1 - y_0)^2]^{1/2}$ is the distance of closest approach of their centers, measured along the $x$ axis. Approximations to the eigenfunctions $\psi_n$ and the eigenvalues $\lambda_n$ can be found by discretizing Eq. (8), which converts it to a real-symmetric matrix eigenvalue problem. The eigenfunctions (taken to be real) can be normalized so that

$$\int [\psi_n(y_1)]^2 dy_1 = 1. \tag{9}$$

In this and subsequent equations, the limits of the $y$ integration are $-h/2$ and $h/2$, the same as in Eq. (8).

Equilibrium expectation values, such as those needed for the quantities $S_n$ defined in (7), can be expressed as integrals involving the eigenfunction $\psi_1$, which corresponds to the largest eigenvalue $\lambda_1$. We illustrate this for the calculation of $S_1$ below.

Here $S_1$ is the expectation value of $\exp(ik_x[x_1 - x_0] + ik_y[y_1 - y_0])$, which is a function of $y_0$, $y_1$, and the gap $s$ between disks 0 and 1, defined by

$$s + \sigma_{1,0} \equiv x_1 - x_0. \tag{10}$$

From the results of Ref. [9], the probability distribution for the variables $y_0$, $y_1$, and $s$ is proportional to

$$\psi_1(y_1)e^{-\beta f[s+\sigma_{1,0}]}\psi_1(y_0).$$

Accordingly, $S_1$ is given by

$$\begin{aligned} S_1 &= \langle e^{ik_x(s+\sigma_{1,0})+ik_y(y_1-y_0)}\rangle \\ &= \frac{\int \psi_1(y_1)\int\int_0^\infty e^{(ik_x-\beta f)(s+\sigma_{1,0})+ik_y(y_1-y_0)}\psi_1(y_0)dsdy_0dy_1}{\int \psi_1(y_1)\int\int_0^\infty e^{-\beta f(s+\sigma_{1,0})}\psi_1(y_0)dsdy_0dy_1}. \end{aligned} \tag{11}$$

After completing the integrals with respect to $s$ and using the eigenvalue equation (8) and the normalization condition (9) to simplify the denominator, we obtain

$$\begin{aligned} S_1 &= \int \psi_1(y_1)\left\{\frac{\beta f}{\lambda_1(\beta f - ik_x)}\right. \\ &\quad \left.\times \int e^{(ik_x-\beta f)\sigma_{1,0}+ik_y(y_1-y_0)}\psi_1(y_0)dy_0\right\}dy_1 \\ &\equiv \int \psi_1\hat{S}\psi_1 dy_1, \end{aligned} \tag{12}$$

in which the bracketed expression in the first line defines the action of the integral operator $\hat{S}$ on $\psi_1$. More generally, for $n \geqslant 1$ one can write

$$S_n = \int \psi_1\hat{S}^n\psi_1 dy_1, \tag{13}$$

so the sum in Eq. (6) becomes

$$\sum_{n=1}^{\infty} S_n = \sum_{n=1}^{\infty}\int \psi_1\hat{S}^n\psi_1 dy_1 = \int \psi_1\hat{S}\phi\, dy_1, \tag{14}$$

where $\phi$ is the solution of

$$\phi = \psi_1 + \hat{S}\phi, \tag{15}$$

which is a Fredholm equation of the second kind. Given the function $\psi_1$ found by solving the discretized equation (8), the calculation of $\phi$ requires only the solution of the set of linear equations obtained by discretizing Eq. (15). Finally, in terms of $\psi_1(y_1)$ and $\phi(y_1)$, the structure factor is given by

$$S(k_x,k_y) = 1 + 2\,\mathrm{Re}\int \psi_1\hat{S}\phi\, dy_1, \tag{16}$$

which depends on $k_x$ and $k_y$ via $\phi$ and the operator $\hat{S}$.

As indicated above, Eqs. (8) and (15) can be solved by discretization. For all but the smallest values of $\beta f\sigma$, the function $\psi_1$ is concentrated near the walls and it is sampled at smaller intervals in those regions, to keep the dimension of the matrices relatively small. To implement this nonuniform

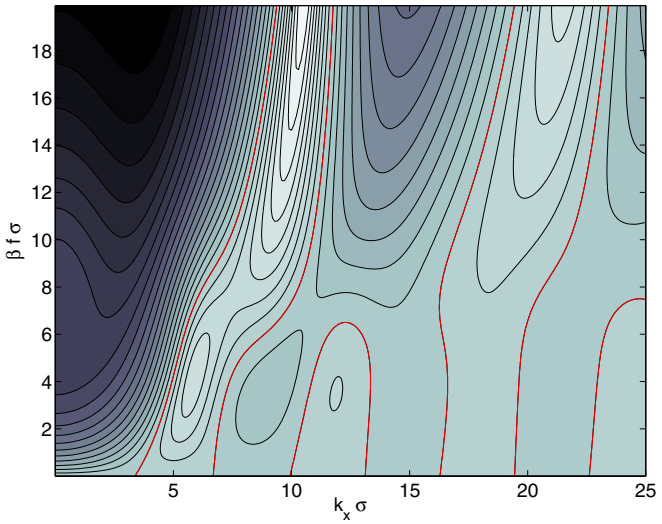


FIG. 3. Structure factor $S(k_x,k_y=0)$ as a function of $\beta f\sigma$ and $k_x\sigma$ for the narrow-channel system with $h=\sqrt{3}\sigma/2$. The position of the first peak in $S$ (near $k_x\sigma=6$ for $\beta f\sigma=4$) changes rapidly for $\beta f\sigma$ in the range 6.5–8, following the change in periodicity that accompanies the growth of zigzag order. Adjacent contours are spaced by 0.1 in $\log_{10} S$ and contour lines with $S=1$ are marked in red.

sampling we make the change of variable

$$u(y)=\frac{\sinh(\alpha\beta f y)}{\sinh(\alpha\beta f h/2)}, \tag{17}$$

where $\alpha=\frac{1}{2}h/\sqrt{\sigma^2-h^2}$ and the values of $u$ are taken to be uniformly spaced in the interval $[-1,1]$. The symmetry of the transfer matrix is preserved by solving Eq. (8) for the function $[dy/du]^{1/2}\psi_1$, rather than $\psi_1$. Matrices of dimension $100\times100$ are sufficient to reproduce the results presented in this section.

Numerical results are shown in Figs. 3–7. In Fig. 3, the structure factor is plotted as a function of $\beta f\sigma$ and $k_x$ for

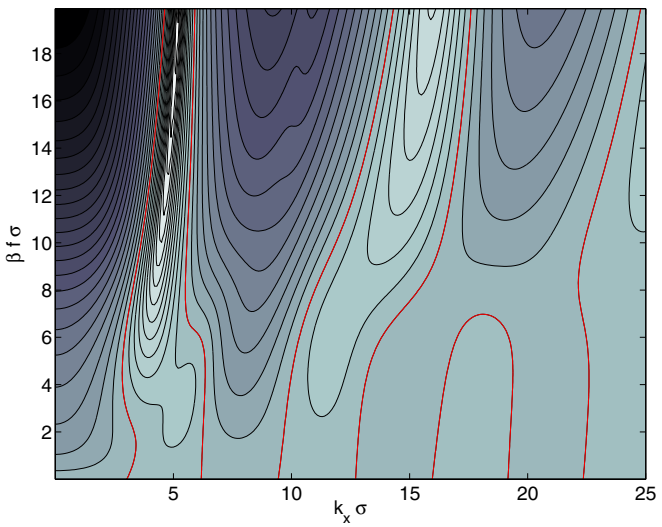


FIG. 4. Structure factor $S(k_x,k_y=\pi/h)$ as a function of $\beta F\sigma$ and $k_x\sigma$ for the narrow-channel system with $h=\sqrt{3}\sigma/2$. A peak near $k_x\sigma=4$ grows rapidly for $\beta f\sigma>4$, consistent with the growth of zigzag correlations. Contour lines are described in the caption to Fig. 3.

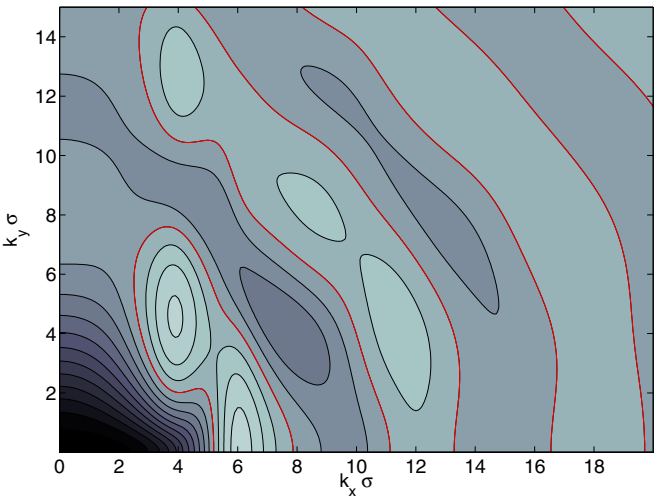


FIG. 5. Structure factor $S(k_x,k_y)$ for $\beta f\sigma=5$ for the narrow-channel system with $h=\sqrt{3}\sigma/2$. Contour lines are described in the caption to Fig. 3.

the case $k_y=0$. For $k_y=0$, the structure factor is sensitive only to correlations in the $y$-averaged density. Zigzag order is growing rapidly for $\beta f\sigma$ in the range 6.5–8 and this can be seen in Fig. 3 as a rapid change in the nature of the first maximum with respect to $k_x$. For very small values of $f$, the oscillations in $S(k_x,k_y=0)$ are small and (much as for a low-density gas of hard rods) their presence is due to the discontinuity of the pair distribution function $g(r)$ at $r=\sigma$. However, as $f$ increases, a new peak emerges and rapidly becomes dominant. Its position reflects the changing spatial periodicity in the $x$ direction: For $\beta f\sigma\to\infty$, the peak approaches $k_x=4\pi/\sigma$, which can be understood as $2\pi/(\sigma/2)$, where $\sigma/2$ is the spatial period of the $y$-averaged density in this limit.

Figure 4 shows the evolution of the structure factor for the case $k_y=\pi/h$, where the value of $k_y$ has been chosen to better illustrate the growth of zigzag order. Note that when $\beta f\sigma$ is

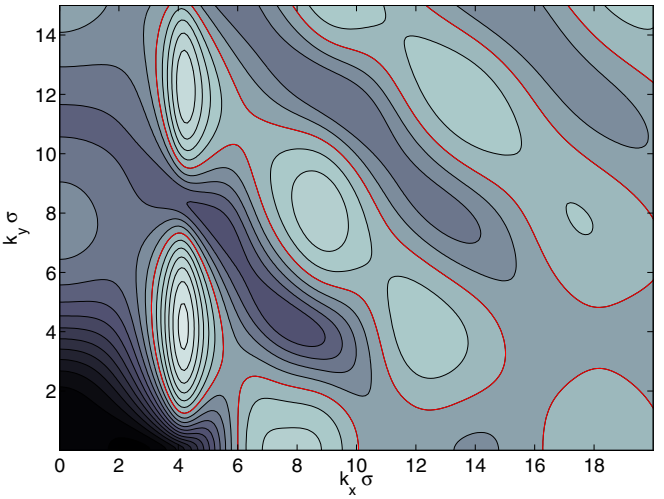


FIG. 6. Structure factor $S(k_x,k_y)$ for $\beta f\sigma=7.5$ for the narrow-channel system with $h=\sqrt{3}\sigma/2$. Contour lines are described in the caption to Fig. 3.

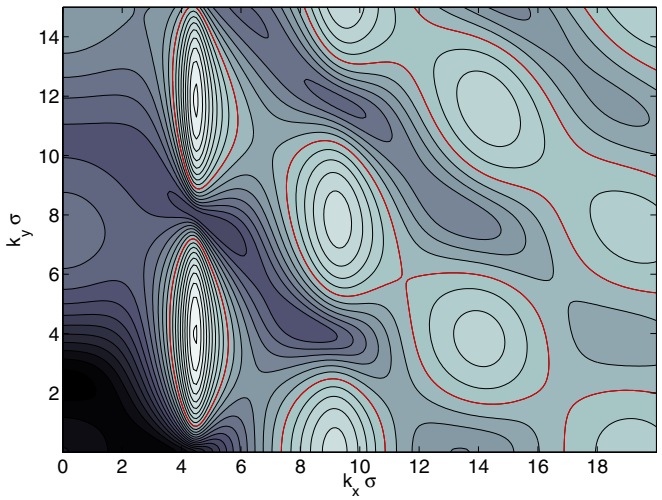


FIG. 7. Structure factor $S(k_x,k_y)$ for $\beta f\sigma = 10$ for the narrow-channel system with $h = \sqrt{3}\sigma/2$. Contour lines are described in the caption to Fig. 3.

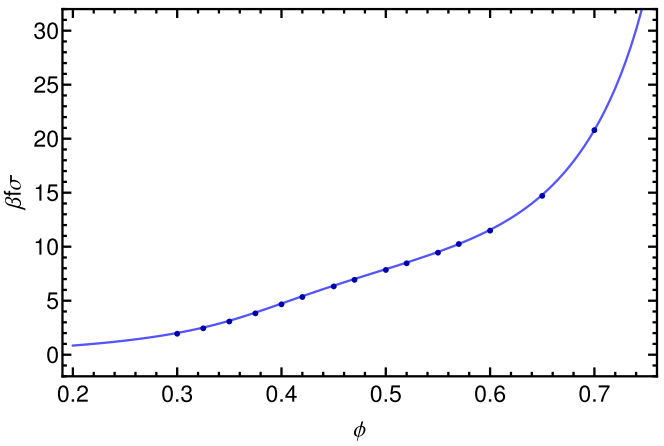


FIG. 8. Equation of state $\beta f\sigma$ versus $\phi$ for the narrow-channel system with $h = \sqrt{3}\sigma/2$. The solid line shows the equation of state calculated from the transfer-matrix results of Ref. [6], while the data points were obtained from long-time simulations of $N = 10\,000$ disks.

large, nearest-neighbor disks are separated by $\Delta x \approx \sigma/2$ along the channel and by $\Delta y \approx \pm h$ in the transverse direction. For $k_y = \pi/h$, the nearest neighbors will scatter in phase when $k_x \Delta x \approx \pi$, i.e., for $k_x \approx 2\pi/\sigma$. This scattering results in a peak in the structure factor that is clearly visible in Fig. 4. The peak first appears near $k_x\sigma = 4$ for $\beta f\sigma \approx 4$. It strengthens as $\beta f\sigma$ increases and it eventually approaches $k_x\sigma = 2\pi$.

Figures 5–7 show the structure factor for three values of the force for which $S(k_x,k_y)$ is changing most rapidly: $\beta f\sigma = 5$, 7.5, and 10. The maxima in $S$ grow and become narrower (in the $k_x$ direction) as $f$ increases and the zigzag correlations strengthen. For very large $f$, the widths of the peaks decrease as $(\beta f\sigma)^{-2}$. We note that this $f$ dependence of the peak width is the same as is found for a one-dimensional gas of hard rods, whose structure factor was derived analytically by Zernike and Prins [23].

## III. TIME-DEPENDENT BEHAVIOR

In order to study time-dependent effects we have used event-driven molecular dynamics based upon the code referred to in Ref. [24]; the speed of the program was improved by using the fact that in our narrow-channel system only nearest-neighbor disks can collide. The initial state from which the system evolves was created by means of the Lubachevsky-Stillinger algorithm [25], starting from a random configuration of small disks. Their diameters were slowly increased to the desired value during the course of a simulation, which preceded the long runs used to study dynamics in the equilibrated system.

The force $f$ along the channel was computed by using a virial formula. Suppose that at the instant of collision between two disks, the $x$ separation of their centers is $\Delta x(c) > 0$, where $c$ labels the collision. The $x$ component of the momentum transferred from the disk at smaller $x$ to the disk at larger $x$ is a positive quantity $\Delta p_x(c) > 0$. With the values of $\Delta x(c)$ and $\Delta p_x(c)$ determined by simulation, the average longitudinal force can be found from

$$fL = \frac{N}{\beta} + \frac{1}{\tau_{\rm sim}} \sum_c \Delta x(c) \Delta p_x(c), \tag{18}$$

where the sum includes all disk-disk collisions $c$ that occur during the simulation time $\tau_{\rm sim}$.

All of our simulations were performed with $N = 10\,000$, $h = \sqrt{3}/2$, and $\beta = \sigma = m = 1$, where $m$ is the mass of a disk. To check their accuracy we calculated the equation of state and compared it with the results of the exact transfer-matrix calculation [6], as shown in Fig. 8.

The agreement is excellent up to $\phi = 0.65$. There is a discrepancy at $\phi = 0.70$ (but too small to be visible in the figure) as at this packing fraction the time scale for equilibration $\tau_D$ is becoming comparable to our simulation time.

### A. Time scales

To see the emergence of caging behavior it is convenient to study

$$\tilde{\Delta}^2(t) = \frac{1}{N} \sum_{i=1}^{N} \frac{1}{\langle |y_i(t) - y_i(0)|^{-2} \rangle}, \tag{19}$$

where the angular brackets indicate an average over runs with different initial states. Though it appears unnatural at first sight, this quantity was introduced in Ref. [26] to minimize the contribution of rattlers. The ability of rattlers to move a distance of $O(\sigma)$ tends to dominate the mean-square displacements at short times $t$. We have a similar problem here in that a few disks that border gaps are able to cross from one side of the channel without hindrance. In Fig. 9 one can see the emergence of a plateau as $\phi$ increases from 0.45 to 0.50, which suggests that caging of the disks is setting in as the zigzag order develops around $\phi_d$. It was in Ref. [1] that $\phi_d \approx 0.48$ was first identified as the onset point for activated dynamics.

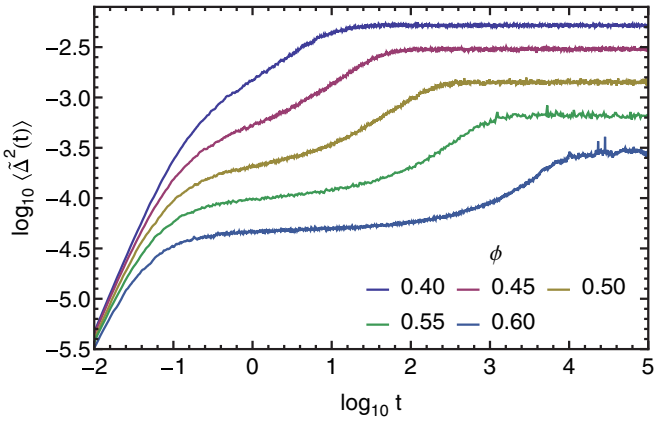


FIG. 9. Time dependence of the mean-square displacements (in units of $\sigma^2$) of 10 000 disks defined via Eq. (19), a quantity that was introduced in Ref. [26] to minimize the contribution from the most mobile disks. The results for the various packing fractions $\phi$ that were studied are averaged over 20 independent equilibrated trajectories. Time is in units of $(\beta m\sigma^2)^{1/2}$.

It is easier to understand the behavior of the unmodified mean-square displacement $\Delta^2(t)$ as defined in Eq. (4). However, Fig. 10 shows that for this quantity the plateau is only clearly visible at values of $\phi$ above 0.60, which is well into the density regime where the dynamics are activated [1,6].

Some of the features on display in Fig. 10 include the following.

(i) There is a final long-time limit: In the limit $t \to \infty$, $\Delta^2(t)$ reaches a finite value. (In three dimensions in the same limit, the mean-square displacement of a particle increases without limit linearly with $t$.) From its definition, $\Delta^2 = \langle y_i^2(t) + y_i^2(0) - 2y_i(t)y_i(0)\rangle$; the last term in angular brackets gives $2R(t)$, which tends to zero in the long-time limit, so $\Delta^2$ tends to $2\langle y_i^2\rangle$, a quantity that is close to $2(h/2)^2$ in the limit of large $f$ when the disks are mostly pushed to the sides of the channel.

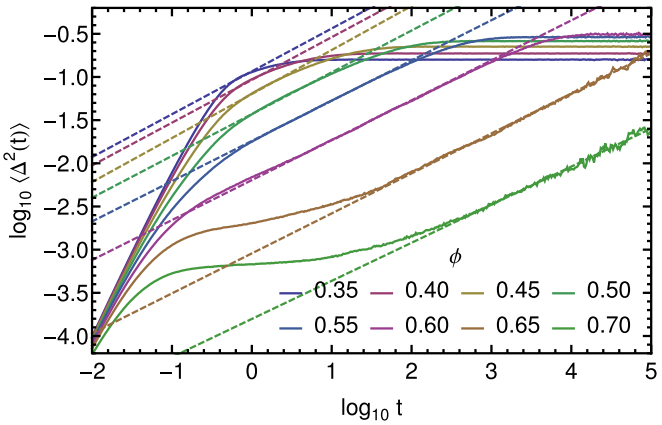


FIG. 10. Time dependence of the mean-square displacements (in units of $\sigma^2$) for trajectories of 10 000 disks at varying packing fractions $\phi$. Time is in units of $(\beta m\sigma^2)^{1/2}$. The dashed lines fit the central regions where the gradient is approximately 0.5, indicating a process of relaxation that is dominated by the diffusion of defects, as suggested in [6] as a mechanism for the $\alpha$ relaxation. For $\phi \gtrsim 0.60$ a plateau is seen to form between the small-$t$ ballistic and large-$t$ diffusive regimes. The plateau corresponds to disks becoming trapped in cages formed by their neighboring disks, which require cooperative motion to break. At very long times $\Delta^2(t)$ tends to a constant value $2\langle y_i^2\rangle$.

(ii) For small $t$, $\Delta^2(t)$ increases as $t^2$; i.e., the motion is ballistic. This regime is larger at smaller values of $\phi$, for which the gaps between disks are larger.

(iii) A shoulder begins to form around $\phi \sim 0.60$ and develops into a clearly visible plateau for $\phi \gtrsim 0.65$. This is a clear analog of the caging effect seen in three dimensions. It sets in at higher packing fractions than $\phi_d \approx 0.48$, the packing fraction at which the growing zigzag order results in the dynamics becoming activated.

(iv) Beyond the glassy plateau for $\phi \geqslant 0.60$ and above the ballistic regime for $\phi \leqslant 0.60$, there is a time scale $\tau$ beyond which a power-law dependence on $t$ sets in, $\Delta^2(t) \propto t^{1/2}$. This dependence on $t$ is due to the slow diffusion of defects in the zigzag arrangement of disks.

We can explain some of these features in greater detail. While activated dynamics may set in around a packing fraction $\phi \approx 0.48$, some disks still find at this density that they can easily cross the channel, and it is not until a packing fraction of 0.60 that the numbers of these "rattling" disks become negligible. The plateau represents a clear caging effect and it lasts for a time $\tau$, the time it typically takes for a disk to cross from one side of the channel to the other by the transition state mechanism depicted in Fig. 2. Once the zigzag order sets in, the motion of the defects as in Fig. 2 dominates the behavior of most of the disks. However, at packing fractions around 0.48 there are still some disks that can travel from one side of the channel to the other with little hindrance from their neighbors. (A similar observation was made in Ref. [4].) Their contribution to $\tilde{\Delta}^2(t)$, defined in Eq. (19), is small, which enables one to see the emergence of the caging behavior in it at lower packing fractions than for $\Delta^2(t)$.

The time scale $\tau$ for a defect to move as shown in Fig. 2 was studied numerically in Ref. [1] and explained using transition state theory in Refs. [6,27]. At high packing fractions

$$\tau \sim \tau_0 \exp(\beta f \Delta_b), \tag{20}$$

where $\tau_0$ is of the order of a disk collision time. The argument of the exponential in Eq. (20) can be understood from Fig. 2: $\beta f \Delta_b$ is the work done against the piston in creating the extra length $\Delta_b$ in the system, which allows the defect to move. In Ref. [6] it was shown that this extra length was $\Delta_b = \sqrt{4\sigma^2 - h^2} - \sigma - \sqrt{\sigma - h^2}$, which can also be understood by inspection of Fig. 2. The plateau visible at larger packing fractions in Fig. 10 will end on the time scale $\tau$.

We now turn to the details of the diffusive behavior, indicated by the dashed lines in Fig. 10. The mean-square displacement $\Delta^2(t)$ increases as $\langle y_i(t)y_i(0)\rangle$ goes to zero. The crossing of disks from one side to the other of the channel is what drives this correlation function to zero. Figure 2 shows that this happens where there are defects in the zigzag arrangement of the disks. Let $\theta$ be the concentration of defects so that the number of defects is $N\theta$. This number is readily determined in numerical work using the procedure given in Ref. [3]. Figure 11 shows $\theta$ as a function of packing

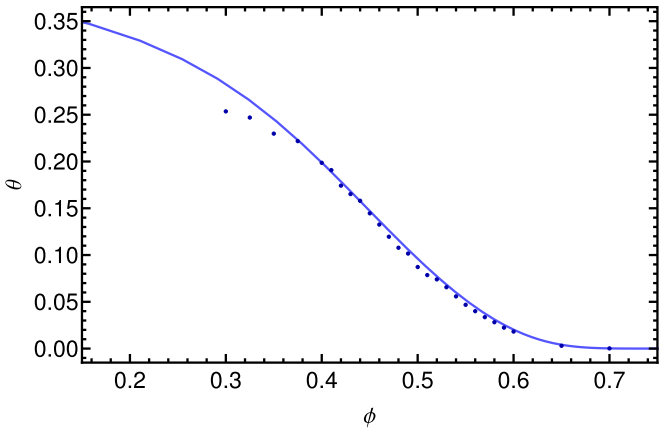


FIG. 11. Variation of the defect density $\theta$ with packing fraction $\phi$. The points give the observed defect densities in our simulations and the dashed line is the approximate theoretical relation predicted in Ref. [6]. The approximate relation is expected to improve in the limit of $\phi \to \phi_{\max}$, which is seen here in the increased agreement between simulation and analytic values as $\phi$ increases, with the exception of the result for $\phi = 0.7$ where we found 4 times more defects than expected. This discrepancy is most likely due to poor equilibration as the trajectory was simulated for a time period much shorter than its relaxation time. Relaxation times $\tau_D$ are shown in Fig. 12.

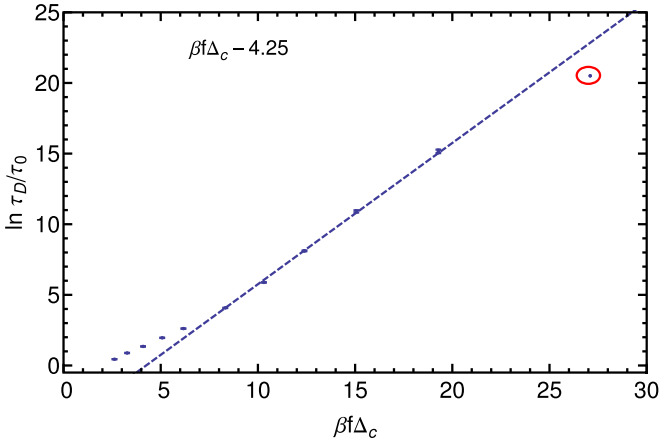


FIG. 12. Rapid increase in the $\tau_D$-relaxation times with longitudinal force $f$, obtained by assigning a linear fit to the diffusive region of the mean-square displacements (see Fig. 10) and extrapolating to find the time where it meets the analytic final values of $\Delta^2(t)$. The dashed line fits the exponential trend predicted by Eq. (21) that is $\ln \tau_D/\tau_0 \sim \beta f \Delta_c$ and becomes an increasingly better fit as $f$ becomes large, i.e., in the limit $\phi \to \phi_{\max}$. The circled data point, corresponding to $\phi = 0.7$, deviates from this trend: As noted in the caption to Fig. 11, the system failed to reach equilibrium for this value of $\phi$.

fraction $\phi$ obtained from the simulations and compared with the analytical approach of Ref. [6], which becomes exact at large packing fractions.

As time increases the number of disks flipped by the diffusion of the defects will be of order $N\theta\sqrt{Dt}$, where $D$ is the diffusion coefficient of a defect. It was argued in Ref. [6] that at large $f$, $D\tau_D \sim 1/\theta^2$. Then

$$\tau_D \sim \tau_0 \exp(\beta f \Delta_c), \tag{21}$$

where $\Delta_c = \sqrt{4\sigma^2 - h^2} + \sigma - 3\sqrt{\sigma^2 - h^2}$. The physical significance of the time scale $\tau_D$ is that it is the time scale on which diffusing defects meet and annihilate [6]. It appears to be the longest timescale in the system: the time scale for full equilibration. Note that in the diffusive region

$$\Delta^2(t) \sim h^2\sqrt{t/\tau_D}. \tag{22}$$

By extending the dashed lines in Fig. 10 to the points where they meet the analytic final values of $\Delta^2(t)$ we can estimate values for $\tau_D$. Values of $\tau_D/\tau_0$ are plotted in Fig. 12. The collision time scale $\tau_0$ was estimated from the mean collision rate per disk determined from our simulations, i.e.,

$$\frac{1}{\tau_0} = \frac{n_c}{N\tau_{\text{sim}}}, \tag{23}$$

where $n_c$ is the total number of collisions that occurred during the simulation time $\tau_{\text{sim}}$. The agreement with the prediction (21) is satisfactory for the results shown in Fig. 12.

We have also used the results shown in Fig. 10 to obtain the diffusion coefficient for defects. At high density, the diffusion coefficient should be related to $\tau$ by $D\tau_0 \sim \tau_0/\tau$ and so might be expected to provide confirmation of Eq. (20). To find $D$, we make use of (22) in the form

$$\Delta^2(t) \sim h^2\theta\sqrt{Dt}. \tag{24}$$

Extrapolation of the dashed lines in Fig. 10 back to $t = 1$ gives, via (24), an estimate of $\theta\sqrt{D}$. This in turn provides $D$ when we make use of the values of $\theta$ found from our simulations. Results for $D\tau_0$ obtained in this way are plotted in Fig. 13. The results show a significant departure from Eq. (20), but there are several reasons why we might expect our procedure to give poor results for the densities of interest here. First we note that for the smaller values of the packing fraction the lines of slope 0.5 in Fig. 10 are not very convincing fits to the data: The linear portions of the curves are very short. Second, the mean spacing of defects given by $1/\theta$ is not large (see Fig. 11) for $\phi$ in the range 0.4–0.6: Interactions between defects may well modify the diffusion coefficient significantly, leading to a

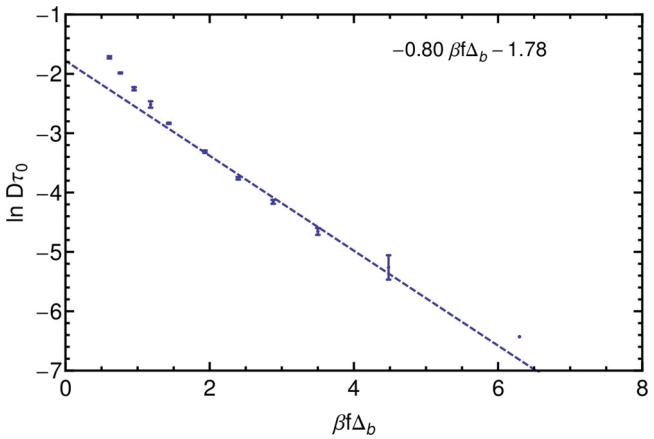


FIG. 13. Variation of diffusion constant $D \propto 1/\tau$ with longitudinal force $f$ using the $y$ intercept of linear fits to the diffusive regions shown in Fig. 10. The dashed line fits the exponential trend predicted by Eq. (20), $\ln \tau/\tau_0 \sim \beta f \Delta_b$.

$\theta$-dependent factor in the relation $D \sim 1/\tau$. Finally, as shown in Ref. [6], $\theta$ itself is not a simple exponential function of $\beta f \sigma$ at these moderate values of $\phi$, but instead can be calculated quite accurately (see Fig. 11) from a law of mass action. Thus, even if $\tau$ has the activated form (20), it is not certain that this can be ascertained from our calculation of $D$ at the moderate densities accessible via our simulation.

Fortunately, it is not necessary to rely on an estimate of the diffusion coefficient to verify the activated behavior of $\tau$. Bowles and Saika-Voivod [1] have made a direct determination of the channel-crossing time from their molecular dynamics simulation. As shown in Ref. [6], their results are in satisfactory agreement with Eq. (20).

Finally, we comment very briefly on the time-dependent correlation function $R(t) = \langle y_i(t) y_i(0) \rangle$, mentioned in Sec. I: $R(t)$ decays to zero because of the diffusion of the defects in the regular zigzag arrangement of disks in the channel. Such a diffusive mechanism has been much studied [18] and leads to a stretched exponential decay $R(t) \sim \exp(-\sqrt{t/\tau_D})$. We have not attempted a direct verification of this behavior of $R(t)$, as it is expected only for very large times $t \gg \tau_D$.

### B. Overlap correlations

We turn now to a study of overlap correlations, which correlate the configuration of the system at time $t$ with a configuration drawn from the equilibrium ensemble at time $t = 0$. Studies of such correlations reveal the existence of dynamical heterogeneities in three-dimensional glass-forming liquids. It is therefore of interest to see whether the system of disks in a channel shows similar behavior. In particular we will make use of the (self-) overlap function

$$Q(t) = \frac{1}{N} \sum_i w[y_i(t), y_i(0)], \tag{25}$$

where $w[y_i(t), y_i(0)] = \frac{1}{2}\{\mathrm{sgn}[y_i(t)]\,\mathrm{sgn}[y_i(0)] + 1\}$ is unity if disk $i$ is on the same side of the channel at times 0 and $t$ and zero otherwise; in the terminology of Ref. [20], this quantity is the *mobility* of disk $i$. Similar overlap functions have been studied in three dimensions: In that case, the overlap $w[\mathbf{r}_i, \mathbf{r}_j]$ has been taken to be 1 if $|\mathbf{r}_i - \mathbf{r}_j| \leqslant 0.3\sigma$ and zero otherwise [14,15,19]. A significant difference between this latter definition and our own is that our overlap function does not depend on the $x$ coordinates of disks. This modification eliminates an effect, specific to our one-dimensional problem, of large fluctuations ($\sim N^{1/2}$) in the $x$ coordinates of disks. These fluctuations can cause the overlap between two configurations to be small even in cases where the configurations would be identical, when described in terms of defects in the zigzag arrangement of disks.

A quantity much studied for three-dimensional systems is the four-point susceptibility $\chi_4(t)$, which is defined in terms of the variance of $Q(t)$ via

$$\chi_4(t)/N = \langle Q(t)^2 \rangle - \langle Q(t) \rangle^2. \tag{26}$$

This has been calculated for our one-dimensional system and is shown in Fig. 14. In three dimensions it reaches a maximum on the time scale $\tau_\alpha$ and subsequently decreases towards zero, but for our system there is no decay back to zero. This difference between dimensions $d = 3$ and $d = 1$ was discussed previously in Ref. [28] and can be understood qualitatively as follows. In three dimensions the self-overlap $w[\mathbf{r}_i(t), \mathbf{r}_i(0)]$ becomes small and is likely to remain small once a sphere has escaped from its cage; it follows that the fluctuations in $Q(t)$ will also be small for times that are long enough for most of the spheres to have escaped from their cages. This argument does not apply to our system of disks in a channel because a disk can cross the channel any number of times, so $w[y_i(t), y_i(0)]$ is a fluctuating quantity of order unity. For any value of $t$, the $y$ coordinates of disks are correlated over a range $\xi$ and are approximately independent over larger distances. From this we expect the contributions to $Q(t)$ from independent regions of size $\xi$ to be fluctuating quantities of order $\xi/N$ for times $t > \tau_D$. If the number of these regions is $m_\xi \sim N/\xi$, we expect

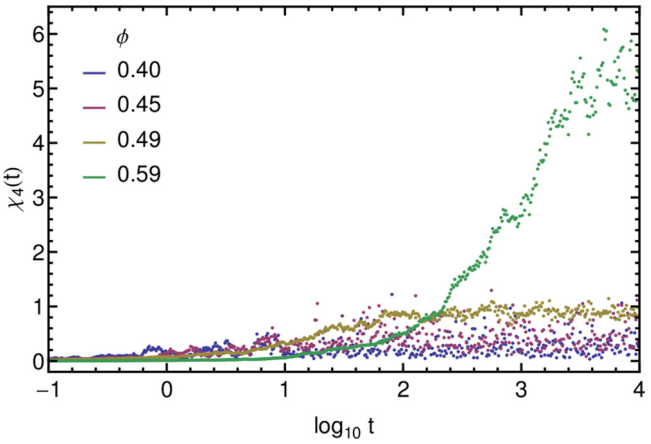


FIG. 14. Four-point susceptibility $\chi_4(t)$, as defined by Eq. (26), as a function of time $t$ for various packing fractions $\phi$. It approaches its largest values at a time corresponding to $\tau_D$.

$$\chi_4/N = \mathrm{Var}\, Q(t) \sim m_\xi (\xi/N)^2, \tag{27}$$

which gives $\chi_4 \sim \xi$ for long times. This result can be refined by using Eq. (2) to evaluate the right-hand side of (26); we obtain

$$\chi_4(t) \approx \xi/4 \tag{28}$$

for $t \gg \tau_D$ and $\xi \gg 1$. The last estimate (28) is consistent with the results shown in Fig. 14 for $\phi = 0.49$ and 0.59, for which $\xi = 3.9$ and 20.9, respectively.

We have also determined the dynamical length scale from the four-point correlation function $\widetilde{S}_4(\kappa_x, t)$ defined as

$$\widetilde{S}_4(\kappa_x, t) = \frac{1}{N} \langle \widetilde{Q}(\kappa_x, t) \widetilde{Q}^*(\kappa_x, t) \rangle, \tag{29}$$

where

$$\widetilde{Q}(\kappa_x, t) = \sum_j e^{-i\kappa_x j} y_j(t) y_j(0) \tag{30}$$

and $\kappa_x = 2\pi m/N$, where $m = 1, 2, \ldots, N-1$. The $\kappa_x$ dependence of $\widetilde{S}_4(\kappa_x, t)$ follows a roughly Lorentzian form, as found in Refs. [15,19], i.e.,

$$\widetilde{S}_4(\kappa_x, t) \approx \frac{A(t)}{1 + \kappa_x^2 \xi_4^2(t)}$$

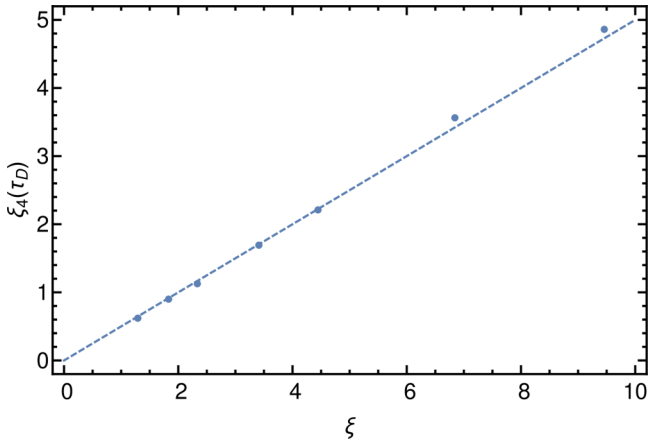


FIG. 15. Plot of the dynamical length scale $\xi_4(\tau_D)$ versus the static length scale $\xi$ of zigzag order. The gradient of the dashed line is 0.5, corresponding to the predicted behavior, Eq. (32).

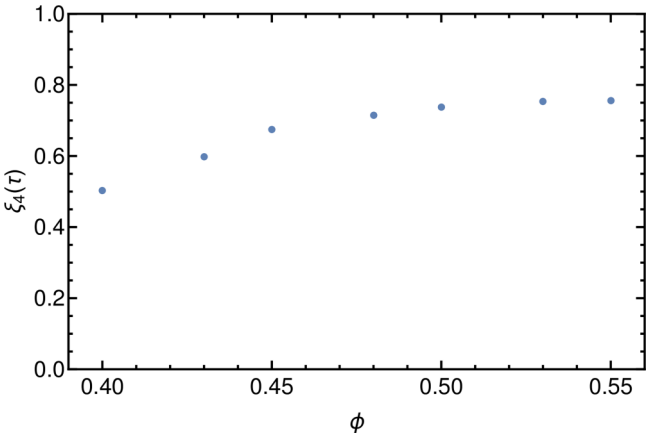


FIG. 16. Plot of the dynamical length scale $\xi_4(\tau)$ versus the packing fraction $\phi$.

for $\kappa_x \neq 0$; the dynamical length scale $\xi_4(t)$ is obtained from a fit to the simulation data.

We present results for $\xi_4(t)$ at two physically significant values of $t$. At $t = \tau_D$ the system has reached equilibrium, so

$$\widetilde{S}_4(\kappa_x, \tau_D) \approx \frac{1}{N} \sum_{p,q} e^{-i\kappa_x(p-q)} \langle y_p y_q \rangle^2. \tag{31}$$

Then, by using Eq. (2), one finds the correlation length

$$\xi_4(\tau_D) \approx \xi/2. \tag{32}$$

Here $\xi$ is the number of disks for which zigzag order persists. This dimensionless quantity is calculated from the two largest eigenvalues $\lambda_1$ and $\lambda_2$ of the integral equation (8), using the expression

$$\xi = 1/\ln(\lambda_1/|\lambda_2|), \tag{33}$$

which follows from the spectral representation of correlation functions, discussed for the case of the Ising model in Sec. 2.2 of Ref. [29] and applied to a system of hard disks in a channel by Varga *et al.* [10]. The results shown in Fig. 15 are in good agreement with the prediction (32).

If we choose for $t$ a value less than the equilibration time $\tau_D$, then $\xi_4(t)$ will be less than $\xi/2$. On the time scale $\tau$, the time for which particles are caged, $\xi_4(\tau)$ is not proportional to $\xi$ and the results in Fig. 16 show it instead to be of order 1 and approximately independent of $\phi$ for $\phi > \phi_d$. This behavior of $\xi_4(\tau)$ is understandable, as on the time scale $\tau$ the active regions are centered on the defects, which involve $O(1)$ disks.

The above studies show that our system has dynamical heterogeneities of the kind expected in the defect-mediated scenario for glassy dynamics [28,30]. In the packing-fraction regime where the dynamics are activated, most of the disks will be largely frozen except those in the vicinity of a defect. The spacing between defects is of order $\xi$, which can become very large. The defects move about and will eventually annihilate with each other. This happens on the time scale $\tau_D$, which is also the time scale on which new pairs of defects are typically nucleated [6].

## IV. CONCLUSION

There are some notable similarities between the behavior of our system of disks in a narrow channel and that found for a fluid of hard spheres in three dimensions. In each of these systems at higher densities the mean-square displacement of particles has a plateau that persists up to the characteristic time for the breaking of cages, $\tau$ or $\tau_\alpha$. Also, in both systems there is a crossover from nonactivated dynamics to activated dynamics as the density increases and caging sets in. In this latter respect, the behavior of these systems is distinctly different from that of a hard-sphere crystal with defects, where the particles are always caged and the diffusion of defects will occur via an activated process.

There are, of course, some important differences. In the channel system, the growing bond-orientational order that we associate with the caging of disks is clearly visible in the structure factor and this is not the case for the three-dimensional glass-forming liquids, where higher-order correlation functions are required to reveal bond-orientational order. The difference here is due to the channel walls, which form part of the cages: Their direction is fixed and so constrains the possible directions of the bonds between nearest-neighbor disks. This can be seen from the top and bottom diagrams in Fig. 2, where only three nearest-neighbor bond directions are possible at $\phi \to \phi_{\max}$.

Another difference appears in the behavior of the dynamical susceptibility $\chi_4(t)$, which, for the channel system, does not tend to zero for $t \to \infty$. We note, however, that this is the expected behavior of $\chi_4(t)$ in defect-mediated models of glassy dynamics in one dimension [28].

We believe that our work strongly supports the common idea [13–17] that glass behavior is a consequence of geometry and the local arrangements around the molecules in the supercooled liquid. Our system is sufficiently simple that we can quantitatively relate its dynamical features to structural features. The three-dimensional problem is much richer and success along these lines is probably only just starting [17].

The caging effects in our system mimic those seen in three dimensions. These are normally modeled by mode-coupling theory [31] and are associated with a genuine dynamical transition, within that approximation. Our system

is effectively one dimensional and is unlikely to have a genuine phase transition. We are skeptical that the features that we see in the dynamics could be explained in any way by mode-coupling arguments. They seem instead to be more naturally explained by dynamical processes associated with the developing structural order in the system. We suspect that the same might be true of three-dimensional systems.

A noteworthy feature of the dynamics of our system of disks is the existence of *two* long timescales $\tau$ and $\tau_D$. In three dimensions, only the analog of $\tau$, which is the cage-breaking time $\tau_\alpha$, is normally discussed. However, in two dimensions a second, much longer, time scale has been revealed in experimental studies of polydisperse colloidal crystals, reported by Tanaka *et al.* [32,33]. In their systems there is a growing length scale $\xi$ for bond-orientational order and their second long timescale $\tau_\xi$ is associated with dynamical correlations on that length scale. This is strikingly similar to what we have found for the case of disks in a channel, where the growing length scale is that of zigzag ordering, which is a form of bond-orientational order. It might, of course, be that the second long timescale is a feature of the dynamics only for one- and two-dimensional systems. One would expect two long timescales to exist in three dimensions if escaping the cage could be associated with moving a defect; the longer timescale would then be associated with the time that the system needs to reach equilibrium via the motion of defects.


[1] R. K. Bowles and I. Saika-Voivod, Phys. Rev. E **73**, 011503 (2006).
[2] M. Z. Yamchi, S. S. Ashwin, and R. K. Bowles, Phys. Rev. Lett. **109**, 225701 (2012).
[3] S. S. Ashwin, M. Z. Yamchi, and R. K. Bowles, Phys. Rev. Lett. **110**, 145701 (2013).
[4] M. Z. Yamchi, S. S. Ashwin, and R. K. Bowles, Phys. Rev. E **91**, 022301 (2015).
[5] S. S. Ashwin and R. K. Bowles, Phys. Rev. Lett. **102**, 235701 (2009).
[6] M. J. Godfrey and M. A. Moore, Phys. Rev. E **89**, 032111 (2014).
[7] M. J. Godfrey and M. A. Moore, Phys. Rev. E **91**, 022120 (2015).
[8] J. A. Barker, Aust. J. Phys. **15**, 127 (1962).
[9] D. A. Kofke and A. J. Post, J. Chem. Phys. **98**, 4853 (1993).
[10] S. Varga, G. Balló, and P. Gurin, J. Stat. Mech. (2011) P11006.
[11] P. Gurin and S. Varga, J. Chem. Phys. **139**, 244708 (2013).
[12] G. Parisi and F. Zamponi, Rev. Mod. Phys. **82**, 789 (2010).
[13] A. Malins, J. Eggers, H. Tanaka, and C. P. Royall, Faraday Discuss. **167**, 405 (2013).
[14] C. P. Royall and S. R. Williams, Phys. Rep. **560**, 1 (2015).
[15] C. P. Royall, A. Malins, A. J. Dunleavy, and R. Pinney, J. Non-Cryst. Solids **407**, 34 (2015).
[16] G. Tarjus, S. A. Kivelson, Z. Nussinov, and P. Viot, J. Phys.: Condens. Matter **17**, R1143 (2005).
[17] E. D. Cubuk, S. S. Schoenholz, J. M. Rieser, B. D. Malone, J. Rottler, D. J. Durian, E. Kaxiras, and A. J. Liu, Phys. Rev. Lett. **114**, 108001 (2015).
[18] S. Redner and K. Kang, J. Phys. A: Math. Gen. **17**, L451 (1984).
[19] N. Lačević, F. W. Starr, T. B. Schrøder, and S. C. Glotzer, J. Chem. Phys. **119**, 7372 (2003).
[20] L. Berthier, Physics **4**, 42 (2011).
[21] J.-P. Bouchaud and G. Biroli, Phys. Rev. B **72**, 064204 (2005).
[22] J. Frenkel, *Kinetic Theory of Liquids* (Oxford University Press, Oxford, 1946).
[23] F. Zernike and J. A. Prins, Z. Phys. **41**, 184 (1927).
[24] M. Skoge, A. Donev, F. H. Stillinger, and S. Torquato, Phys. Rev. E **74**, 041127 (2006).
[25] B. D. Lubachevsky and F. H. Stillinger, J. Stat. Phys. **60**, 561 (1990).
[26] A. Ikeda, L. Berthier, and G. Biroli, J. Chem. Phys. **138**, 12A507 (2013).
[27] M. Barnett-Jones, P. A. Dickinson, M. J. Godfrey, T. Grundy, and M. A. Moore, Phys. Rev. E **88**, 052132 (2013).
[28] C. Toninelli, M. Wyart, L. Berthier, G. Biroli, and J.-P. Bouchaud, Phys. Rev. E **71**, 041505 (2005).
[29] R. J. Baxter, *Exactly Solved Models in Statistical Mechanics* (Academic, New York, 1982).
[30] L. Berthier and G. Biroli, Rev. Mod. Phys. **83**, 587 (2011).
[31] W. Götze and T. Voigtmann, Phys. Rev. E **67**, 021502 (2003).
[32] H. Tanaka, T. Kawasaki, H. Shintani, and K. Watanabe, Nat. Mater. **9**, 324 (2010).
[33] H. Tanaka, Eur. Phys. J. E **35**, 113 (2012).